Nanoscale

Accepted Manuscript

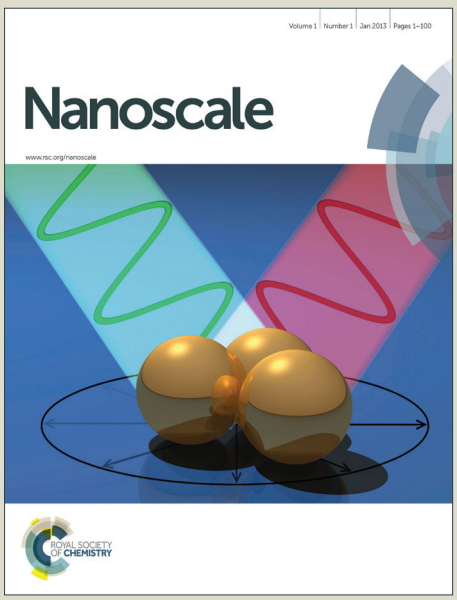

ROYAL SOCIETY OF CHEMISTRY

www.rsc.org/nanoscale

Cite this: DOI: 10.1039/c0xx00000x

www.rsc.org/xxxxxx

ARTICLE TYPE

Au-ZnO Janus Nanoparticles Exhibiting Strong Charge-Transfer-Induced SERS for Recyclable SERS-active Substrates

Liping Liu[a,b], Haitao Yang[*a], Xiao Ren[a], Jin Tang[a], Yongfeng Li[*b], Xiangqun Zhang[a] and Zhaohua Cheng[a]

Received (in XXX, XXX) Xth XXXXXXXXX 20XX, Accepted Xth XXXXXXXXX 20XX
DOI: 10.1039/b000000x

The flower-shaped Au-ZnO Janus nanoparticles have been prepared via the seeding growth and subsequent wet-chemical etching of Au-ZnO core-shell nanoparticles. The etched Au-ZnO Janus nanoparticles have shown a stronger surface-enhanced Raman scattering (SERS) signal of the nontotally symmetric (b_2) vibrational modes of the PATP molecules than Au nanoparticles alone, which is attributed that the chemical enhanced effect of ZnO layer is greatly excited by the localized surface plasmon resonance (LSPR) of Au cores. Further, the mechanism of LSPR-enhanced charge transfer (CT) effect has been proved by the SERS spectra of PATP molecules excited at different laser resources from 325 to 785 nm. Moreover, the photocatalytic experimental results indicated that Au-ZnO Janus nanoparticles are promising to serve as biologically compatible and recyclable SERS-active platforms for different molecular species.

Introduction

Great interests in surface-enhanced Raman scattering (SERS) spectroscopy have been stimulated by one of the most sensitive spectroscopic techniques for label-free chemical and biological detection, possibly extended to the level of single molecule detection sensitivity.[1-4] So far, SERS experiments have been dependent on the use of metals, in particular Ag and Au nanoparticles aggregates or roughened substrates[5-7]. Recently, semiconductor-based SERS has attracted increasing attention due to its broad application prospects not only for developing novel SERS-active substrates, but also broadening the applicability of Raman spectroscopy as a SERS technology to investigate the adsorption problems on semiconductor surfaces.[8,9] For metal nanoparticles, the primary enhancement effect is attributed to electromagnetic (EM) enhancement.[10,11] Whereas for semiconductor nanoparticles, is mostly related to the charge-transfer (CT) between absorbates and semiconductor nanoparticles.[12] In the last few years, many research efforts have been focused on the SERS of metal/semiconductor hybrid nanostructures to pursue more high-efficient SERS-active substrates. In most cases, the metal nanoparticles were anchored on the surfaces of the semiconductors as isolated 'islands' to form composite with a weak interaction between metal nanoparticles and semiconductor nanomaterials. For example, SERS signals of 4-MBA molecules adsorbed on silver-deposited TiO_2 nanoparticles were firstly found, and there was a further enhancement relative to that on pure TiO_2 NPs, which was attributed to the LSPR of the surface-deposited Ag nanoparticles and the TiO_2-to-molecule CT contribution.[13] Subsequently, Ag nanoclusters wrapped ZnO nanowires have shown an effective SERS effect with a large enhancement factor of 3.2×10^8 when used to detect two-photon absorption of chromophore T7 molecules,[14] and Ag nanoparticles-decorated ZnO nanorods have been found as a versatile substrate for SERS not only for common organic molecules but also for label-free protein detection.[15] Further, a strong energy coupling effect located at the metal/semiconductor interface was thought as the major mechanism for the enhanced SERS of Rhodamine 6G (R6G) chromophore absorbed on the ZnO hollow spheres decorated by Ag nanoparticles.[16] This structural drawback results in a high barrier for CT and low biologically compatible due to bare heavy metal. However, few researches on SERS of semiconductor-coated metal nanostructures, as the reverse counterparts of metal-decorated semiconductor, possibly due to the strong limit of EM enhancement effect of the metallic LSPR from semiconductor surrounding.

Herein, we report the synthesis of Au-ZnO Janus nanoparticles by etching Au-ZnO core-shell nanoparticles and the strong SERS effect of such Janus nanoparticles. The observed considerable SERS enhancement of PATP molecule on Au-ZnO Janus nanoparticles compared with that on pure Au and ZnO nanoparticles can be attributed to the ZnO-to-molecule CT contribution which is enhanced by the additional electrons from LSPR of Au nanoparticles to the ZnO surface through the conduction band of ZnO nanoparticles. Moreover, the photocatalytic experimental results showed that Au-ZnO Janus nanoparticles are characterized by high reproducibility after visible-light-assisted cleaning which makes them promising as biologically compatible and recyclable SERS-active platforms for different molecular species.

Experiments

10 nm gold nanoparticles as seeds were firstly prepared by the reduction of gold chloride ($HAuCl_4 \cdot 4H_2O$) with oleylamine. Typically, 1 mmol of $HAuCl_4 \cdot 4H_2O$ and 15 mmol of oleylamine were mixed with 50 mL toluene in a 100 mL flask. Under Ar

protection, the mixture was heated to 80 °C and kept at this temperature for 8 h with magnetic stirring. The Au nanoparticles were collected by centrifugation and redispersed in hexane. Au-ZnO core-shell nanoparticles were prepared by a seeding growth method. Zinc acetate dihydrate (1 mmol), oleylamine (3 mL), and dodecanol (6 mL) were mixed and heated until a clear solution formed under a flow of Ar gas. After 10 mg Au nanoparticles were added to that mixed solution, the above solution was further heated to 230 °C and hatched for 1 h. After cooling to room temperature, the generated products were separated from solution by centrifugation and washed with acetone several times. Finally, the product was dispersed in hexane with a concentration of 7 mg/mL. The preparation of ZnO nanoparticles was similar to the synthesis procedure of Au-ZnO core-shell nanoparticles except the adding of Au seeds.

Au-ZnO nanoparticles were etched by acetic acid diluted with ethanol (pH∼3). 20 mL acetic acid solution and 20 mg Au-ZnO nanoparticles were mixed under continuous stirring at room temperature. Samples were extracted at different etching time until the color of the mixture changed from purple to blue.

Au, ZnO, Au-ZnO core-shell nanoparticles, and etched Au-ZnO nanoparticles were deposited on the SiO_2/Si substrate for SERS measurement, respectively. A total of 100 μL of hexane dispersion of the hydrophobic nanoparticles was dropped onto the 1 × 1 cm^2 SiO_2/Si wafer with a 300 nm SiO_2 top layer and dried under ambient conditions. Then, this Si wafer was put into a 5 mL beaker containing 1 mL of 1 × 10^{-5} M PATP (p-aminothiophenol) ethanol solution. After 12 hours, the nanoparticles covered Si wafer was washed three times with ethanol and dried in air.

The photocatalytic activities of the etched Au-ZnO Janus nanoparticles were evaluated by the photocatalytic degradation of Rhodamine B (RhB) in an aqueous solution under visible-light irradiation. A 300 W Xe lamp with a 400 nm cut-off filter was used as the visible light source. Prior to visible-light exposure, 100 ml of RhB (2mg/L) and 10 mg of Au-ZnO Janus nanoparticle powder were magnetically stirred in the dark for 2 hours to equilibrate the absorption and desorption of dye molecules.

Characterization

Powder X-ray diffraction (XRD) data was collected on a D2 PHASER X-ray difffractometer (Cu K^{α} radiation, λ= 0.154 nm). The morphology and structure properties of samples were investigated by transmission electron microscope (TEM, JEM-2100F with operation voltage 200 kV). UV-visible spectra were recorded with a Varian Cary 5000 ultraviolet-visible spectrophotometer. Raman spectra were obtained with a Renishaw Raman system model in Via-Reflex spectrometer and a LabRam HR 800 spectrometer of HORIBA Co.. The 325 nm radiation from a He-Cd laser, 532 nm radiation from a solid-state laser, 632.8 nm from a He-Ne laser and 785 nm radiation from semiconductor-state laser were used as exciting source.

Results and Discussion

Figure 1a shows the low resolution TEM image of the as-prepared Au-ZnO core-shell nanoparticles. It can be observed that each Au cores are coated by several ZnO nanopyramids, forming

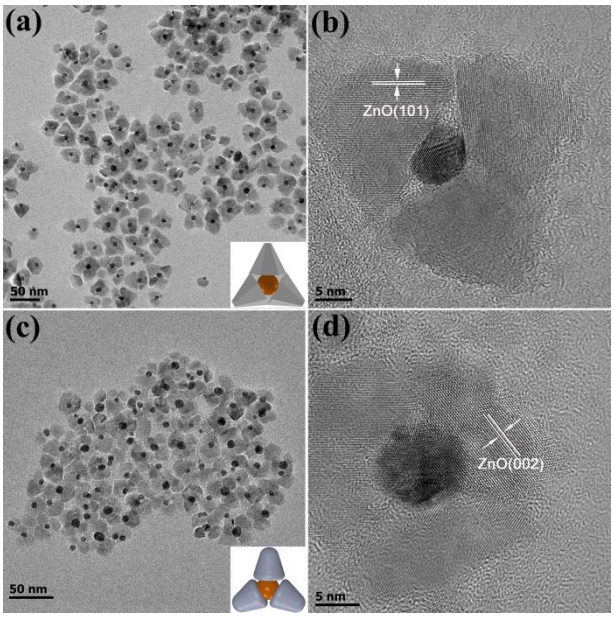

Fig. 1 (a) TEM and (b) HRTEM images of Au-ZnO nanopyramids; (c) TEM and (d) HRTEM images of etched Au-ZnO Janus nanoparticle.

multipyramid nanostructures. The sizes of Au cores are about 10 nm and the lengths of the side edge of ZnO nanopyramids are in the range of 20∼30 nm. The HRTEM image (Fig. 1b) of Au-ZnO core-shell nanoparticles presents the lattice fringes belonging to the (101) plane of wurtzite-type ZnO. Interestingly, it can be observed that the Au cores are located on the centers of the hexagonal basal surface, i.e. the {0001} polar plane of ZnO nanoparticles, which leads to the basal surface of ZnO preferentially grows on Au seeds because of the lower interface energy for the polar/metal interface.[17] Meanwhile, the relatively large lattice mismatch (∼5%), which is the lowest mismatch between (101) facets of ZnO and (111) facets of Au, required the free electrons from the Au to compensate for the charge induced by the polarized plane at the interface when ZnO starts nucleation on the Au seeds. The polar solvent, dodecanol, can provide charges to compensate for the apparent electron density loss of Au seeds allowing nucleation on multiple facets of Au cores and formation of core-shell nanoparticles.[18] The time-evolution TEM images of the Au-ZnO core-shell nanoparticles etched in acetic acid are shown in Fig. S1. Obviously, the ZnO shell has vanished gradually with etching time. After the etching treatment of 6 minutes, ZnO nanopyramids (Fig. 1c) turn into the nanoflower-like shape and the sizes of ZnO nanopyramids reduce to ∼10 nm. Two or several flower-shaped ZnO nanoparticles still decorate at each Au core. Furthermore, the ZnO nanoparticles become rough and parts of Au seeds surface are exposed as shown in the TEM image (Fig. 1 d). In addition, the XRD pattern of etched Au–ZnO Janus nanoparticles is the same as the Au-ZnO core-shell nanopyramids (Fig. S2). It demonstrates that no impurity or crystalline phase has been induced in the sample after etching.

Figure 2 shows UV-vis absorption spectra of the Au seeds, Au-ZnO nanopyramids, etched Au-ZnO Janus nanoparticles before and after absorbing PATP molecules, respectively. The absorption spectra of Au nanoparticles exhibit an absorption band with a maximum absorption wavelength (λ_{max}) of about 522±8

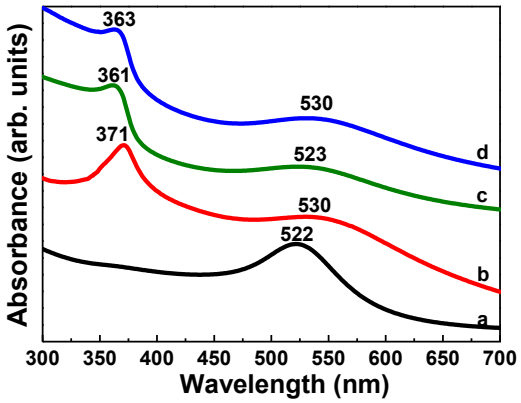

Fig. 2 UV-vis absorption spectra of (a) the Au nanoparticles, (b) the Au-ZnO core-shell nanoparticles, (c) the etched Au-ZnO Janus nanoparticles, and (d) the etched Au-ZnO Janus nanoparticles after absorbing PATP.

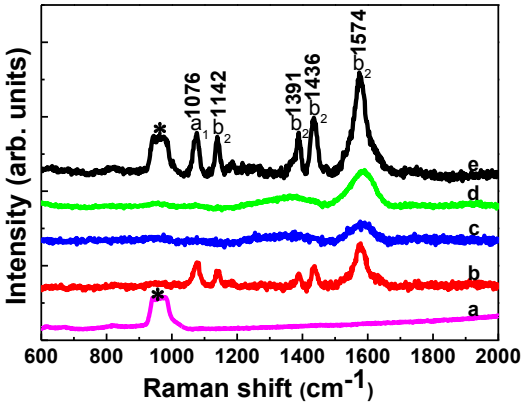

Fig. 3 SERS spectra of PATP molecules absorbed on (a) the ZnO nanoaprticles, (b) the Au nanoaprticles, (c) the Au-ZnO nanopyramids, (d) the etched Au-ZnO nanoparticles with 3 minutes, and (e) the etched Au-ZnO Janus particles with 6 minutes with 532 nm laser excitation. The broad peak marked by the star (*) is from Si.

nm, which are caused by LSPR of gold nanoparticles. After coating with ZnO nanopyramids, the characteristic gold plasma resonance peak (Fig. 2b) red-shifts from 522 to 530 nm against pure Au nanoparticles, reflecting Au nanoparticles surrounded by high-refractive-index ZnO shells.[19] Whereas, after etching the ZnO nanopyramids, the λ_{max} shifts back to 523 nm, due to the increasing surface plasmon sensitivity with the reduced volume fraction of ZnO shell based on the Mie theory.[20] Therefore the variation of dielectric surrounding can largely change the LSPR behavior of Au cores. Besides the LSPR absorption band of gold cores, the absorption band of ZnO shows a blue-shift from 371nm of the Au-ZnO core-shell nanoparticles to about 360nm of the etched Au-ZnO Janus nanoparticles due to the decrease size of ZnO shell related to confinement effects.[21] It can also be founded that, after the etched Au-ZnO Janus nanoparticles adsorb the PATP molecules (Fig. 2c,d), the absorption band of 361 nm shifts to 363 nm. These changes are attributed to the electronic interaction of PATP molecules and ZnO nanoparticles.

Figure 3 shows the Raman spectra of PATP molecules adsorbed on the different nanostructures at a laser excitation wavelength of 532 nm. The predominant bands in the spectrum of PATP solid powders (as shown in Figure S3) are located at 1593, 1177, and 1086 cm^{-1}, which are the a_1 modes of the PATP molecule.[22] The a_1 and b_2 species of the PATP molecule are in-plane modes, and a_2 and b_1 species are out of-plane modes of benzene ring. Whereas the strong bands are observed at 1574, 1436, 1391, and 1142 cm^{-1} in the Au nanoparticles absorbed PATP in Fig. 3b, which are assigned to the nontotally symmetric b_2 vibrational modes of the PATP molecule.[23] Except for 1077 cm^{-1}, the other a_1 modes Raman bands are not observed, which means that the b_2 vibrational modes of the PATP molecule on the gold nanoparticles were selectively enhanced. According to the surface-selection role of the EM model,[24] the totally symmetric (a_1) modes should be most strongly enhanced and the SERS enhancement for nontotally symmetric modes with C_{2v} symmetry also should include b_1 or a_2. So CT enhancement mechanism dominantly contributes to the SERS of PATP molecule.[23] In the pure ZnO nanoparticles, no Raman peak is obtained (Fig. 3a) except a rectangle-shaped peak corresponding to Si substrate. In the Au-ZnO core-shell nanoparticles, two broad bands of ~1398 and ~1580 cm^{-1} are observed (as shown in Fig. 3c), which are assigned to the b_2 modes of the PATP molecule. It is reasonable to conclude that the weak SERS signal is from the chemical enhancement mechanism of ZnO nanoparticles. Because the EM and CT enhanced effect of Au cores to PATP molecule are inhibited by the thick ZnO shell, whereas the ZnO-to-molecule CT contribution which is enhanced by the additional electrons from LSPR of Au cores to the ZnO surface through the conduction band of ZnO nanoparticles. However, after etching treatment for 3 minutes, these two broad bands of ~1398 and ~1580 cm^{-1} becomes much more intense (Fig. 3d). Moreover, after etching 6 minutes, the a_1 modes Raman band at 1076 cm^{-1} and the strong b_2 modes Raman bands at 1574, 1436, 1391, and 1142 cm^{-1} of PATP molecule are all observed in the Raman spectrum of the etched Au-ZnO Janus nanoparticles absorbed PATP molecules as shown in Fig. 3e. The Au-ZnO Janus nanoparticles with 6-minute-etching treatment, with the decreasing ZnO dielectric surrounding and partly exposure of Au core surfaces, have a stronger enhanced effect than those with 3-minute-etching treatment. By comparing curves b and e in Fig. 3, it can be found that the intensity ratio of all four b_2 modes Raman peaks to the a_1 modes peak (1076cm^{-1}) on the etched Au-ZnO Janus nanoparticles is 2~3 times larger than the ratio on the Au nanoparticles, which indicates that the etched Au-ZnO Janus nanoparticles have a higher CT enhancement effect than Au nanoparticles. Since CT mechanism dominantly contributes to the enhancement of the b_2 modes Raman bands of PATP, it can reasonably be concluded that the enhanced LSPR effect of Au cores from the decreasing dielectric surrounding majorly improve the CT enhancement effect.

In order to further reveal the mechanism of enhanced Raman spectra of label molecules on the etched Au-ZnO Janus nanoparticles, the SERS of PATP molecules were measured using 325 nm, 532 nm, 633 nm and 785 nm radiation as the excitation source, respectively (as shown in Fig. 4). Using the 325 nm excitation source, only two weak broad Raman peaks at 1076 cm^{-1} and 1620 cm^{-1} related to a_1 mode are observed. The SERS spectrum using 633 nm laser excitation is much similar to the 532 nm case with a difference in lower intensity of 1574 cm^{-1}

peak. In the 785 nm case, all peaks corresponding to a_1 and b_2 modes also appear with an extremely low intensity of 1436, 1391,

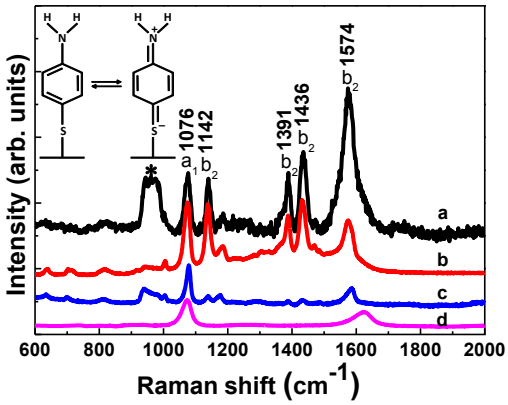

Fig. 4 SERS spectra of PATP molecules adsorbed on the etched Au-ZnO Janus nanoparticles at (a) 532 nm excitation, (b) 632.8 nm excitation, (c) 785 nm excitation, and (d) 325 nm excitation. The broad peak marked by the star (*) is from Si.

and 1142 cm^{-1} peaks, which are strong in the 532nm and 633nm cases. And the relative intensity of b_2/a_1(1076 cm^{-1}) modes peaks using 532 nm laser excitation is the highest among those. These can be attributed to the low LSPR intensity of Au cores excited under some excitation sources at a wavelength far from the 520 nm of the Au plasmon band, which can't strongly accelerate the CT enhancement effects of ZnO nanoparticles.

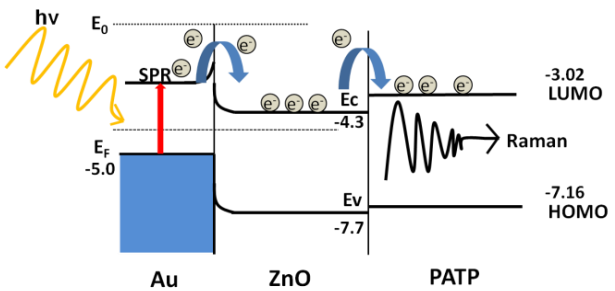

Fig. 5 The schematics of energy alignments mechanism of the etched Au-ZnO/PATP assembly and the SPR generated electron transfer mechanism.

Furthermore, PATP molecules usually interact electrostatically or covalently with nanoparticles in quinonoid forms[25] (as shown in the inset of Fig. 4), which generated an exactly asymmetric metal-semiconductor-molecule system. Since no noticeable difference in the frequencies of the a_1 modes was observed in all four spectra, the bonding geometries between the PATP molecule and nanoparticles have no change in different exciting resources. Therefore, it is reasonable to conclude that the strong electronic interactions between the PATP molecules and nanoparticles are mainly responsible for the selective enhancement of b_2 modes through the Herzberg–Teller coupling.[12] Since the workfunction of Au (≈5.0 eV)[26] is lower than that of ZnO (≈5.2 eV)[27], additional electrons from LSPR of Au cores get transferred to the conduction band of ZnO shell except for the 325 nm excitation. Subsequently, dynamic CT could occur through coupling with the vibrations of the bridging molecules to easily transfer an electron to an excited unfilled level of PATP. Accordingly, the selective enhancement of the b_2 modes of the PATP molecules is an indicative of such a CT process[28] and the 'donor–bridge–acceptor' system is suitable to represent the CT model of the Au-ZnO Janus nanoparticle system, which is schematically plotted to show the energy alignment mechanism in Fig. 5.

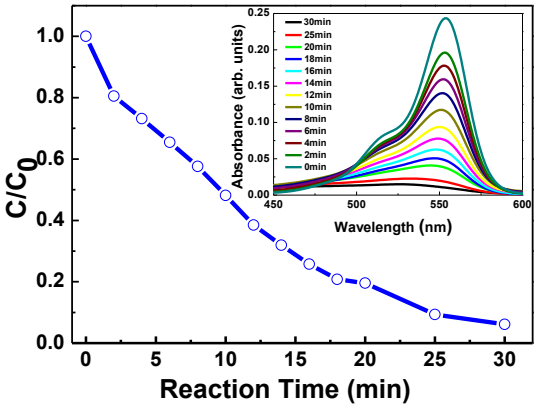

Fig. 6 Photocatalytic performance of rhodamine B under visible light irradiation.

The photocatalytic activities of the etched Au-ZnO Janus nanoparticles were evaluated by the photocatalytic degradation of Rhodamine B (RhB) in an aqueous solution under visible light irradiation. Figure 6 shows the photocatalytic degradation of RhB with the etched Au-ZnO Janus nanoparticles under the visible-light irradiation. It can be observed that RhB (2 mg/L) were completely degraded within 30 min. The photocatalytic experimental results indicated that Au-ZnO Janus nanoparticles are promising to serve as biologically compatible and recyclable SERS-active platforms for different molecular species.

Conclusions

In summary, the Au-ZnO Janus nanoparticles with flower shaped morphology have been prepared via the etching treatment of Au-ZnO core-shell nanoparticles. The etched Au-ZnO Janus nanoparticles as SERS substrates for detection of PATP molecules have shown a stronger SERS signal than Au nanoparticles using a 532 nm laser excitation. The obvious SERS enhancement of the b_2 vibrational mode Raman peaks of the PATP molecules absorbed on the Au-ZnO Janus nanoparticles reveals that CT effect of ZnO is greatly enhanced by the LSPR of Au cores. Further, the mechanism of LSPR-enhanced CT effect has been proved by the SERS spectra of PATP molecules excited at different Laser resources from 325 to 785 nm. Moreover, the photocatalytic experimental results showed that Au-ZnO Janus nanoparticles are characterized by high reproducibility after visible-light-assisted cleaning which make them promising as biologically compatible and recyclable SERS-active platforms for different molecular species.

Acknowledgments

This work was supported by National Nature Science Foundation of China (Grant No. 11274370 and 51471185) and the National Basic Research Program of China (Grant No. 2012CB933102 and

2011CB921801).

Notes and references

[a] *Beijing National Laboratory for Condensed Matter Physics, Institute of Physics, Chinese Academy of Sciences, Beijing 100190, P. R. China; E-mail: htyang@iphy.ac.cn*

[b] *State Key Laboratory of Heavy Oil Processing, China University of Petroleum, Beijing 102249, P. R. China; E-mail: yfli@cup.edu.cn*

† Electronic Supplementary Information (ESI) available: [details of any supplementary information available should be included here]. See DOI: 10.1039/b000000x/

1 N. H. Kim, S. J. Lee and K. Kim, *Chem.Commun*., 2003, 724-725.
2 Y. Liu, D. G. Li and S. H. Sun, *J. Mater. Chem.*, 2011, **21**, 12579.
3 J. Theiss, P. Pavaskar, P. M. Echternach, R. E. Muller and S. B. Cronin, *Nano Lett.*, 2010, **10**, 2749-2754.
4 T. Jin, S. J. Guo, J. L. Zuo and S. H. Sun, *Nanoscale*, 2013, **5**, 160-163.
5 S. Y. Lee, S. H. Kim, M. P. Kim, H. C. Jeon, H. Kang, H. J. Kim, B. J. Kim and S. M. Yang, *Chem. Mater*., 2013, **25**, 2421-2426.
6 T. X. Tan, C. G. Tian, Z. Y. Ren, J. Yang, Y. J. Chen, L. Sun, Z. T. Li, A. P. Wu, J. Yin and H. G. Fu, *Phys. Chem. Chem. Phys.*, 2013, **15**, 21034-21042.
7 A. J. Wilson and K. A. Willets, *Nano Lett.*, 2014, **14**, 939-945.
8 X. X. Zou, R. Silva, X. X. Huang, J. F. Al-Sharab and T. Asefa, *Chem.Commun*., 2013, **49**, 382-384.
9 C. Qiu, Y. Bao, N. L. Netzer and C. Y. Jiang, *J. Mater. Chem. A*, 2013, **1**, 8790.
10 Y. C. Lai, W. X. Pan, D. G. Zhang and J. H. Zhan, *Nanoscale*, 2011, **3**, 2134-2137.
11 Y. Bu and S. Lee, *Appl. Mater. Interfaces*, 2012, **4**, 3923-3931.
12 A. Musumeci, D. Gosztola, T. Schiller, N. M. Dimitrijevic, V. Mujica, D. Martin and T. Rajh, *J. Am. Chem. Soc.*, 2009, **131**, 6040-6041.
13 L. B. Yang, X. Jiang, W. D. Ruan, J. X. Yang, B. Zhao, W. Q. Xu, and J. R. Lombardi, *J. Phys. Chem. C.*, 2009, **113**, 16226.
14 S. Deng, H. M. Fan, X. Zhang, K. P. Loh, C. L. Cheng, C. H. Sow and Y. L. Foo, *Nanotechnology*, 2009, **20**, 175705.
15 W. Song, X. X. Han, L. Chen, Y. M. Yang, B. Tang, W. Ji, W. D. Ruan, W. Q. Xu, B. Zhao and Y. Ozaki, *J. Raman Spectrosc*., 2010, **41**, 907-913.
16 J. Yin, Y. S. Zang, C. Yue, Z. M. Wu, S. T. Wu, J. Li and Z. H. Wu, *J. Mater. Chem.*, 2012, **22**, 7902.
17 A. Figuerola, M. V. Huis, M. Zanella, A. Genovese, S. Marras, A. Falqui, H. W. Zandbergen, R. Cingolani and L. Manna., *Nano Lett.*, 2010, **10**, 3028.
18 H. Yu, M. Chen, P. M. Rice, S. X. Wang, R. L. White, and S. S. Sun, *Nano Lett.*, 2005, **5**, 379.
19 X. F. Wu, H. Y. Song, J. M. Yoon, Y. T. Yu and Y. F. Chen, *Langmuir*, 2009, **25**, 6438-6447.
20 A. C. Templeton, J. J. Pietron, R. W. Murray and P. Mulvaney, *J. Phys.Chem. B*, 2000, **104**, 564-570.
21 Y. Gu, I. L. Kuskovsky, M. Yin, S. O'Brien and G. F. Neumark, *Appl. Phys. Lett.*, 2004, **85**, 3834-3835.
22. L. Gao, P. Diao, L. Tong, T. Zhu and Z. Liu, *Chem. Phys. Chem.*, 2005, **6**, 913-918.
23 M. Osawa, N. Matsuda, K. Yoshii and I. Uchida, *J. Phys. Chem.*, 1994, **98**, 12702-12707.
24 M. Moskovits and J. S. Suh, *J. Phys. Chem.*, 1984, **88**, 5526-5530.
25 Q. Zhou, X. W. Li, Q. Fan, X. X. Zhang and J. W. Zheng, *Angew. Chem. Int. Ed.*, 2006, **45**, 3970-3973.
26 I. G. Hill, J. Schwartz and A. Kahn, *Org. Electron.*, 2000, **1**, 5-13.
27 X. D. Bai, E. G. Wang, P. X. Gao and Z. L. Wang, *Nano Lett.*, 2003, **3**, 1147-1150.
28 K. Kim, K. L. Kim and K. S. Shin, *Phys. Chem. Chem. Phys.*, 2013, **15**, 9288-9294.